

An innovative small-scale prototype plant integrating a solar dish concentrator with a molten salt storage system



Sebastiano Turrini ^{a,b,*}, Marco Bettone ^b, Massimo Eccher ^b, Maurizio Grigiante ^c, Antonio Miotello ^b, Roberto S. Brusa ^b

^a Institute for Polymers, Composites and Biomaterials, National Research Council, Piazzale Tecchio 80, I-80125 Napoli, Italy

^b Department of Physics, University of Trento, Via Sommarive 14, I-38123 Povo, TN, Italy

^c Department of Civil, Environmental and Mechanical Engineering, University of Trento, Via Mesiano 77, 38123 Trento, Italy

ARTICLE INFO

Article history:

Received 8 June 2017

Received in revised form

3 February 2018

Accepted 9 February 2018

Available online 12 February 2018

Keywords:

Renewable energy

CSP technology

PDC - energy integration

Energy storage

Energy analysis

ABSTRACT

An innovative plant configuration joining a thermal energy storage device with a 2 kW_{Th} parabolic solar dish collector (PDC) has been designed. The novelty of this small-scale solar plant prototype consists in the use of molten salts (MS) both as fluid carrier and thermal energy storage medium. An eutectic mixture of NaNO₃, NaNO₂ and KNO₃ has been used allowing a 10 kWh energy storage accomplished with two 50-L tanks. An experimental campaign has been planned to test the behavior of each of the assembled components and to provide a preliminary analysis of the plant performances. As first evaluation, the energy efficiency of the system has been calculated in correspondence to selected MS flow rates referred to steady state conditions. This has been achieved by monitoring the MS temperature in correspondence to suitable points of the inlet and outlet sections of the receiver. The preliminary confirmations of this investigation looks promising to integrate the PDC technology within district heating systems for advanced renewable energy exploitations.

© 2018 Elsevier Ltd. All rights reserved.

1. Introduction

The worldwide increasing demand for distributed energy utilities has rapidly enhanced the opportunities for small power plants ranging from a few kW to several MW. Within this perspective, concentrated solar plants (CSP) are likely to play a strategic role in providing high temperatures devices for advanced solar thermal applications [1]. This technology is expected to supersede in the future the low temperature collectors specifically utilized for domestic hot water supply [2,3].

The CSP technology can be classified into four solar thermal systems. This depends on the way they focus the sun rays and on the solution adopted for the receiver, fixed or mobile [4]: parabolic trough collectors (PTC), tower and parabolic dish collectors (TDC, PDC) and linear Fresnel collectors (LFC).

In parabolic trough and linear Fresnel systems, the mirror tracks the sun to focus sunlight along the focal line (line focus) while, in tower and dish systems, the mirror tracks the sun along two axis

(point focus). In linear Fresnel and tower collectors the receiver is fixed while it is mobile in parabolic trough and dish systems.

Looking at the actual state of art of these technologies, PTC represents the most proven CSP application and dominates the global market being installed in more than 80% of the CSP operating plants. Reference is made to [4,5] for a detailed and updated review of PTC plants installed around the world. Tower systems have just started to be introduced in commercial applications while linear Fresnel plants are currently making their transition to the market. Even though they come under a demonstrative level, the PDC technology is considered particularly attractive for the forthcoming distributed energy market scenario. Moving from these encouraging perspectives, several theoretical and experimental efforts have been developed to address the PDC applications to small and large industries [6–11]. Within this contest, Dish-Stirling technology appears particularly suitable to exploit these opportunities looking at the near-term markets including, as main assets identified by the developers of this technology, remote and grid connected power jointly with end-of-line power conditioning applications [12–14].

Although renewable energies are universally encouraged due to their sustainability advantages and their impact in limiting the

* Corresponding author. Department of Physics, University of Trento, Via Sommarive 14, I-38123 Povo, TN, Italy.

E-mail address: s.turrini@unitn.it (S. Turrini).

Nomenclature

P_D	concentrated solar radiation power [W]
I_{dir}	direct solar radiation [W/m^2]
η_D	parabolic dish combined optical efficiency [-]
A_D	parabolic dish projected area [m^2]
P_R	power absorbed by the molten salt mixture [W]
m_{MS}	molten salt mass flow rate [kg/s]
Q_{MS}	molten salt flow rate [l/min]
C_{MS}	molten salt heat capacity [$\text{J}/(\text{kg K})$]
ρ_{MS}	molten salt density [kg/m^3]
T_{OUT}	temperature of the molten salt mixture at the outlet of the receiver [$^\circ\text{C}$]
T_{IN}	temperature of the molten salt mixture at the inlet of the receiver [$^\circ\text{C}$]
η_{REC}	receiver efficiency [-]
$U_{\eta_{REC}}$	uncertainty of receiver efficiency [-]
$U_{Q_{MS}}$	uncertainty of molten salt mixture flow [m^3/s]
$U_{T_{IN}}$	uncertainty of temperature at the inlet of the receiver [$^\circ\text{C}$]
$U_{T_{OUT}}$	uncertainty of temperature at the outlet of the receiver [$^\circ\text{C}$]
$U_{I_{dir}}$	uncertainty of direct solar irradiation [W/m^2]

greenhouse gas emissions, there is a mismatch between most of the renewable energy supply and the final users demand. To reduce this time mismatch the CSP systems have been integrated with suitable thermal energy storage (TES) devices. TES technology provides a distinct advantage with respect to other renewable energies such as wind and photovoltaic. Also the use of batteries for electrical energy storage has not proven to be economically viable [15]. The use of thermal storage offers the following advantages: mitigating short fluctuations during transient weather conditions; shifting the generation period from peak hours of solar insulation to peak hours of power demand; extending the generation period when solar is not available. Three options have attracted the attention for TES technology: sensible heat storage, latent storage and thermochemical storage. In sensible TES devices the energy is stored/released by raising/lowering the temperature of the storage medium in either a solid or liquid. Latent storage option takes advantage of large latent heat that can be stored/released by changing the phase of the so called phase change materials (PCMs). In thermochemical storage the energy is stored by means of reversible sorption process or chemical reactions. This last technology is still at a very early stage and most of the adopted solutions have been tested only on laboratory scale [16]. Even though on latent heat storage several experiences have been carried out over the past decade [17,18], no commercial PCMs storage systems have been used in utility-scale CSP applications. Only sensible TES is applied and commercially deployed for integration with PTC and TDC systems [19,20]. Looking at the state of art of sensible TES, molten salts (MS) have significantly emerged as high temperature working fluids (HTF) to substitute common synthetic oil for both their enhanced key properties and comparable costs. The ternary mixtures of NaNO_2 , NaNO_3 and KNO_3 , utilized also within this work and commonly known as Hitec [21], are able to withstand a temperature limit over 500°C and present a desirable freezing temperature in the range $120\text{--}140^\circ\text{C}$. Recent studies estimate that the use of MS can reduce the storage cost up to 43% and the cost of the global solar plant up to 15% compared to those configurations involving Therminol VP-1 [22,23]. In utility-scale CSP plants, the

adoption of two tanks for MS storage represents the most commonly storage technique. Usually the MS are used both as storage medium and as HTF [24]. In particular, the adoption of the direct storage approach has been used on both parabolic trough and tower plants. For a detailed analysis of this configuration, reference is made to the Archimede PTC built in Italy [25] and the Solar Tower plant realized in California [26]. This solution has also been adopted for the experimental prototype plant investigated in this study. It consists of a small dish collector coupled with a two tanks TES configuration involving the use of MS both as direct storage medium and HTF as well. This study details in particular the component design scheme, the construction procedures and includes also the presentation of the results referred to a preliminary tests campaign.

The limited budget availability has oriented the choice to a small solar concentration plant. The selection of the PDC technology has been motivated by considering some features of this technology when compared with the consolidated PTC and LFC options:

- the PDC collectors are the most efficient since they always point the sun;
- accordingly to the goodness of the mirrors, PDC allows to reach concentration ratio higher than 2000. This enhances both the energy absorption efficiency and the power conversion;
- these collectors can be used as stand-alone configurations or included on existing plants;
- this technology looks particularly attractive to be integrated within the next generation of solar district energy plants.

Although the experimental investigations of this study are still in progress, the adopted configuration introduces the following significant novelties:

- this is the first example of a small-scale MS dish collector coupled with a TES configuration at the moment adopted only for big PTC plants. A very similar realization can be referred only to US patent 7299633 B2 [27];
- the adopted design configuration includes the transport and the storage of the thermal power by making use of suitable devices positioned at ground level. This solution, at the Authors knowledge, has never been tested before for small scale PDC configurations;
- this study demonstrates the feasibility of integrating small scale CSP with innovative MS storage devices. The adopted solution looks particularly attractive since it allows a more flexible use of MS as HTF.

This last point is worth to note because, in addition to power generation, there are a lot of potential applications working at high temperatures. Reference can be made to the direct usage of thermal energy in food industries and dedicated chemical processes involving both high temperature conditions and normal ranges as required for conventional air conditioning applications [28]. Looking at renewable energy chain value, innovative applications could also include pre-treatment processes like torrefaction and fast pyrolysis. These technologies seem promising in converting biomass into upgraded lignocellulosic materials and bio-oil by involving, as heating carriers, fluids working in the medium temperature range from 250° to 550° [29].

Further, by changing the flow rate of the working fluid, pipes diameter and tanks capacity, the proposed system can be scaled and adapted to PDC having different sizes. With respect to the direct utilization of the power available at the focus of the collector, the proposed configuration could offer two major advantages: 1) the output of the system is not strongly affected by transients in

solar input so that higher efficiencies can be expected [30]; 2) there aren't any size or weight restrictions in the storage design since it can in any case be positioned at ground level.

In this work the performances of the plant are limited to some case tests referred to selected working conditions. An extended experimental campaign is planned and will be specifically oriented to test the performances of each of the plant components. Looking at the organization of the paper, the first part details the design purposes of the adopted plant configuration together with a detailed description of the main components. The second part presents the results of a preliminary test campaign including the evaluation of the global plant efficiency achieved in correspondence to suitable molten salt flow rates, although for limited range conditions.

2. Solar collector

The molten salt system was combined with the solar dish prototype developed at the University of Trento. This collector is based on an easy and innovative process to manufacture parabolic mirrors [31]. The collector design and the characterization of its optical performances are described in detail in Ref. [32]. This prototype was previously used to conduct experiments regarding dense-array photovoltaic receivers [33,34].

Here we briefly report its main characteristics and the configuration used during the molten-salt system testing.

The collector was designed to be constructed with modular parabolic sectors, each having 15° aperture and 0.8 m² surface: a full parabolic dish, 5 m in diameter, would be made by 24 sectors with an overall projection area of about 20 m². At present, our collector prototype is assembled with three parabolic sectors mounted on a polar-equatorial axis solar tracking support, see Fig. 1. The main rotation axis is parallel to earth rotation axis, while a second regulation is manually adjusted to compensate the solar declination angle ($\pm 23^\circ$ in 1 year). The rotation is run by a Oriental Motor step motor, coupled with a Bonfiglioli 1:10000 gearbox; the

resulting angular speed is 0.004167°/sec.

The characterization of a single module confirmed the good quality of the light-spot, with a Gaussian distribution reaching 95% of the total measured power collected in a circle of 5.8 cm in diameter and a peak concentration ratio of about 870×. The overall collection efficiency was found to be between 0.86 and 0.89 [32].

Another calorimetry measure has provided a 0.8 collection efficiency with the 3 mirrors mounted on the supporting framework, therefore confirming the already tested performances.

3. Description of the system

3.1. Heat transfer and storage fluid

Different liquids were evaluated as heat transfer and storage fluid. Water was rejected due to its low normal boiling point that requires high pressures in the circuit to reach high temperatures. Different mixtures of molten salt and diathermic oils have been considered. Oils have the advantage of being already liquid at ambient temperature thus eliminating the need of pre-heating systems and the risks of solidification due to cold spots into the circuit. However, the highest temperature can reach values around 400 °C [35], and, in case of overheating, fire hazard must be taken into account.

The use of molten salt mixtures has been investigated aiming at achieving temperatures above 500 °C. Further constraints were the low melting point to limit the installation of pre-heating devices and the low price of the adopted mixtures.

A ternary mixture of NaNO₂, NaNO₃ and KNO₃, commonly known as Hitec®, was chosen to fulfill the previous indicated requirements. This fluid was originally developed in the 30's by Dupont and has been largely used in the last 50 years in Molten Salt Breeding Reactors [36]. The main properties of this mixture are summarized in Table 1.

The Hitec® fluid is not considered the best available medium for transferring and storing heat. For example "Solar Salt", a binary



Fig. 1. The solar collector prototype at the University of Trento and the molten salt plant assembled on field. The tanks and pumps block (A), dish collector (B), receiver (C) and pipes (D) are visible.

Table 1
Properties of the Hitec® molten salt mixture [37].

%w NaNO ₂	40
%w NaNO ₃	7
%w KNO ₃	53
Fusion temperature	[°C]
Max temperature	[°C]
Density at 300 °C	[kg/m ³]
Viscosity 300 °C	[kg/(m s)]
Heat capacity at 300 °C	J/(kg K)
Thermal conductivity	[W/(m K)]
Coefficient of expansion	[1/K]
	0.34 10 ⁻³

mixture of NaNO₃ and KNO₃, is suggested as a better solution [37] but it requires a significantly higher temperature to melt. Other mixtures were considered to lower the minimal process temperature but they were rejected for lack of documentation and high costs. For a detailed presentation and description of thermophysical properties of these materials reference is made to [36–40].

3.2. Design of the system

In the present approach, a two-tanks storage system was adopted following the model of big solar farms, as the case of SEGS in California [24]. The molten salt mixture has been used both as heat carrier and storage fluid, following the solution adopted in the Archimede plant of Priolo Gargallo (Italy) [25].

The description of the system is done with reference to the layout shown in Fig. 2.

The first tank (“cold tank” or CT hereafter) contains the mixture at a temperature level around 200 °C to guarantee the liquid state of the salts. Salts in the CT are pumped into the receiver where the exposition to concentrated solar radiation heats them up to about 500 °C. The mixture is then stocked in the second tank (“hot tank”, or HT hereafter). A second pump extracts the liquid from the HT and pushes it toward a heat exchanger and then again into the CT. To keep these two temperatures as constant as possible the flow must be continuously regulated at the two pumping stages according to the measurements of two thermocouples placed at the outlet of the receiver and of the heat exchanger, respectively.

In the present system, since the exploitation of the thermal power was beyond the object of the present work, the heat exchanger was a simple counter-flow pipe exchanger. In future, the plant configuration could be implemented with devices suitable for different applications: steam generation, air heating, heat supply for a chemical reactor, etc.

In order to avoid the solidification of the molten salt mixture in any part of the system, high temperature fiberglass heating tapes are used to trace all the pipes while the plant components are preheated by means of appropriate heating apparatuses. The temperature of each heater is monitored by means of a K-type thermocouple and accordingly regulated.

Pre-heating is necessary at the startup of the system because, even if the molten salt is collected in the CT, part of the mixture will inevitably remain inside the pipes. At present, all these pre-heating elements are electrically powered but a renewable energy source could be implemented in a more advanced design.

The system electronic is managed through a Labview code

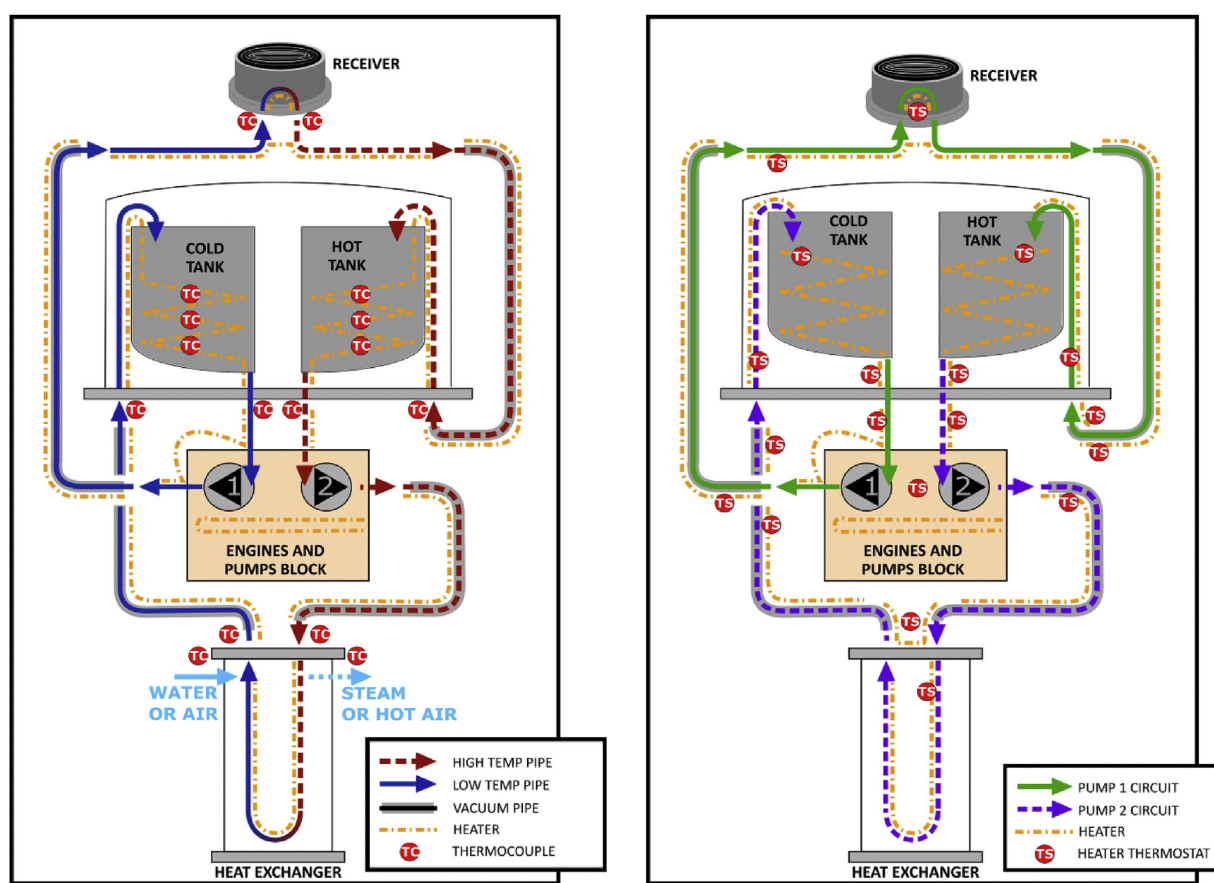


Fig. 2. Schematic diagram of the heat transfer and storage system. On the left: high and low temperature zones and position of thermocouples. On the right: pump 1 and pump 2 circuits and thermostats position.

interfaced with a National Instruments NI USB-6343 card. This software, by means of a single user interface, allows to acquire data from the thermocouples, controls the operation of the pumps, the heaters (with the relative thermostats) and the electronic safety systems.

3.3. Tanks

The tanks (Fig. 3) are made of stainless steel and can contain about 50 L of molten salt (80 kg). The correspondent energy storage E_S can be calculated with Eq. (1):

$$E_S = C_{MS} \cdot \rho_{MS} \cdot \Delta T \cdot V \quad (1)$$

where C_{MS} is the average specific heat capacity of the mixture, ρ_{MS} the density of the mixture, V the volume of the tank. Using parameters of Table 1, the energy storage results in about 10 kWh storage at the temperature of 500 °C and 200 °C for the hot and cold tank, respectively. The two tanks' bodies are externally traced with mineral insulated heating cable; in the cold tank, 6 cartridge heaters, 750 W each, are installed to accomplish the initial melting of the mixture.

In order to monitor the mixture's temperature three k-type thermocouples are mounted at different height levels. As the tanks drain, these thermocouples can also be used as a rudimentary level gauge.

The tanks are placed into a vacuum chamber to reduce convection heat losses. The chamber is supported by a steel structure which also hosts the pumps block and the electrical bay (Fig. 4).

3.4. Motors and pumps

Two pumps are installed, for the CT-receiver-HT circuit and for the HT-heat exchanger-CT circuit, respectively.

Both the pumps are enclosed in a thermally insulated box which can be pre-heated with a heating element up to about 200 °C; a separated box contains 2 motors connected to the pumps (Fig. 5).

The first pump (*cold pump* hereafter) is a Viking pump model C32: a small gear pump made of cast iron with a special packing seal that can bear temperatures up to 350 °C. The pump is connected to a 48 V Sanyo 103-815-7 step motor driven by a Orientalmotor RBD200A-V driver.

The second pump (*hot pump* hereafter), MVV – ASCO VL805, is custom built with AISI 440 B steel and grafoil packing seal to bear temperatures up to 500 °C. The pump is driven by a 3-phase 250 W motor, model ELECTRO ADDA T1A63C-4, coupled with a

BONFIGLIOLI 1:30 worm gear and powered by a OMRON HITACHI 3G3JX-AB004-EF inverter.

The main specifications of the pumps are summarized in Table 2.

Both the pumps cover a flow range from 0.04 to 1 l/min; the rotational speed is measured by means of a BAUMER BHK 16.05A.0500-I2-5 rotary encoder for the step motor and a magnetic speed sensor (4 pulses per round) for the three-phase motor.

3.5. Vacuum pipes

The use of molten salt as heat carrier requires that the temperature is maintained above 150 °C. This means that every single pipe has to be insulated and provided with pre-heaters. For the 2 longest pipes, covering the 5 m length from the tanks to the receiver, and the 2 m pipes connecting the heat exchanger (see Fig. 2), a vacuum design was chosen.

The pipes (Fig. 6) into which molten salt flow are composed by a flexible tube, 6 mm in internal diameter and 9,7 external with two regular 8 mm tubes welded at both ends, and a nominal pressure of 24 bar. These pipes are housed into larger flexible tubes, 32 mm in internal diameter and 41 mm external, with an external braid and a nominal pressure of 144 bar.

Every 20 cm, a spacer built with a copper ring and wire keeps the pipes coaxiality. At one of the ends of the external pipe, a Swagelok® valve is mounted in order to connect the vacuum pump; at the other end, 2 electrical and 2 thermocouple feedthroughs are provided in order to power the heating tapes and regulate the temperature.

The design of the pipes is shown in Fig. 7.

The inner pipe is traced with high temperature heating tape that can stand up to 760 °C. These tapes are highly insulated and built for heavy duty usage. During the setting up of the experimental apparatus no problems attending to the use of the flexible pipes were evidenced. Anyway the use of the heating tape appears laborious in the mounting. A simpler heating method to be implemented in a new version of the system would be the direct heating of the internal tube by Joule effect. This would require the insulation of the internal respect to the external tube at the connections.

3.6. Solar energy receiver

The cavity receiver designed for this experimentation was designed to effectively transfer the energy to the fluid, still being light enough to be placed on the prototypal structure.

In order to increase the contact surface between the salt and the receiver while minimizing the pressure drop, a copper tube 6 mm in diameter was used. The tube approximately 1.20 m long was shaped to form a bowl and welded to a hollow copper cylinder which intercepts part of the concentrated solar radiation (Fig. 8). A k-type thermocouple is attached to this cylinder to monitor the temperature on a single point. This measurement, which provides only an indicative value of the global temperature of the receiver, is used during the preheating to check that the salts melting point has been exceeded.

The manufactured receiver is shown in Fig. 9.

The receiver was chemically oxidized to increase the solar absorption: firstly, the copper was sandblasted to clean the surface, washed with distilled water and dried in air; then the receiver was immersed into a sealed glass container, containing an alkaline solution (0.1 M NaOH) of $K_2S_2O_8$, 0.001M and left still at 70 °C for 60 h. The pH of solution was kept at 13. After this process a black surface was obtained (Fig. 9).

The receiver is housed into a cylindrical steel chamber 115 mm in diameter and 90 mm high externally insulated with mineral

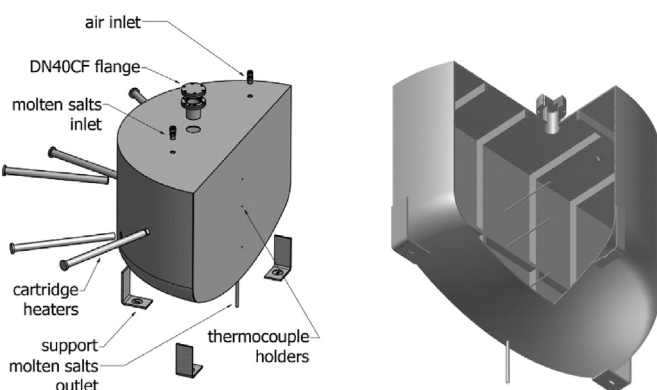


Fig. 3. On the left, cold tank's components. On the right, section view showing the internal reinforcements and the small cylinder holders for the insertion of the thermocouples.



Fig. 4. The two tanks in the open vacuum chamber: steel support (A), pump block (B), electrical bay (C) and heat exchanger (D) are also visible.

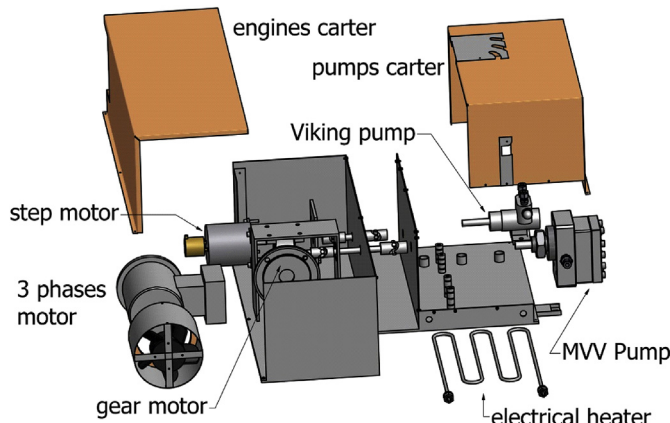


Fig. 5. Exploded view of the pump block.

Table 2
Pumps' specifications.

	Viking C32	MVV ASCO VL805
Circuit	CT → Receiver → HT	HT → HX → CT
Pump Type	gear pump	gear pump
Material	cast iron (body), carbon steel, nitr alloy, carbon graphite	AISI 440B grafoil
Maximum temperature	300 °C	550 °C
Flow Range	0.04 ÷ 1 l/min	0.04 ÷ 1 l/min

wool and aluminum sheets (Fig. 10). The final external dimensions are 16 × 11 cm (diameter x height); the weight of the assembly is 4.5 kg.

Two more thermocouples are employed to monitor the temperature of the molten salt at the inlet and outlet of the receiver. These thermocouples, as shown in Fig. 11, are housed in 2 steel cylinders which are connected to a Swagelok® three-way connector



Fig. 6. The 2 m pipe that connects the hot pump to the heat exchanger.

at the back of the receiver in order to be in direct contact with the Hitec® flow.

4. Experimental method

The described system was completely assembled on field in a dedicated outdoor area (Fig. 1) and every single component was thoroughly tested. In order to measure the increase in molten salt temperature when the receiver was placed in the focus of the solar collector and exposed to concentrated solar radiation, a simplified version of the circuit was used. As shown in Fig. 12, the system was arranged using the cold tank and the cold pump only to circulate the molten salt mixture. The remaining part of the circuit (hot tank, hot pump and heat exchanger) was bypassed to avoid the complexity related to further control and pre-heating.

4.1. Measuring instrumentation

Temperatures at the inlet and outlet of the receiver, as well as ambient temperature, were measured by means of k-type thermocouples connected to an Agilent 34970A datalogger; direct solar radiation was measured with a Kipp & Zonen CHP1 pyrheliometer connected to an Agilent 34410 digital multimeter.

The molten salt flow was controlled through adjustment of the cold pump speed which is measured by a Baumer BHK

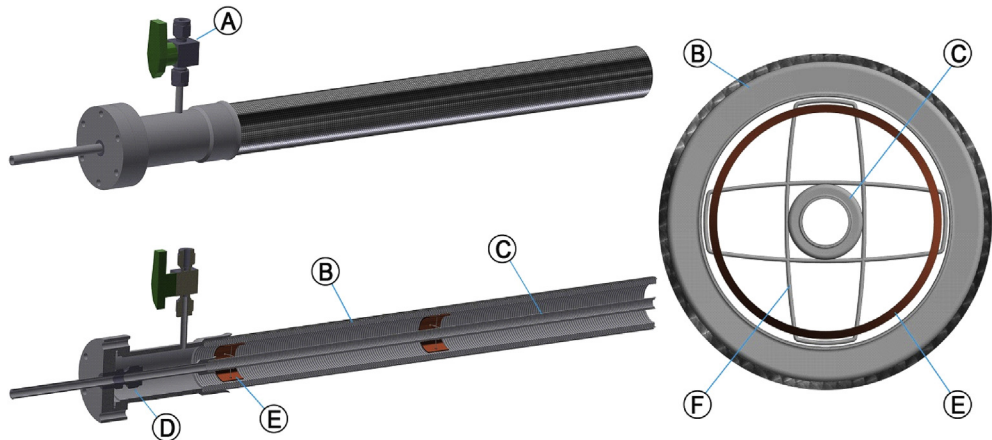


Fig. 7. Cad drawing of the vacuum pipes design. The Swagelok® Valve (A), external tube (B), internal tube (C), Swagelok® weld fitting (D), copper spacer (E) and wire (F) are visible.

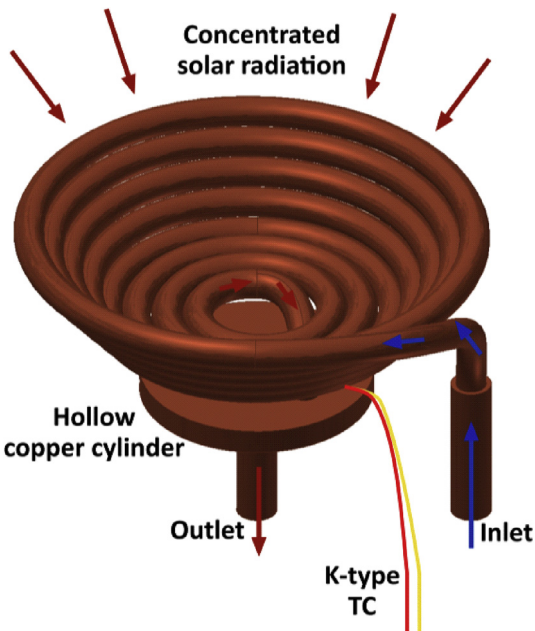


Fig. 8. 3-d model of the cavity receiver. A thermocouple is attached to the copper cylinder under the spiraled tube.

16.05A.0500-I2-5 rotary encoder to keep into account any possible discrepancy between the desired speed and the actual movement of the step motor.

4.2. Measuring procedure

The system was preheated up to about 290 °C, to avoid any possible solidification of the molten salt mixture. At the beginning of the process the molten salt flow was set at 0.3 l/min; the collector was then aligned to the sun while keeping a protective shield raised in front of the receiver. After steady state conditions for the salt flow were reached, the receiver and the input and output pipes preheaters were switched off and the flow was regulated at 0.5 l/min. Successively the shield was lowered to expose the receiver to the concentrated solar radiation. The thermocouple inside the receiver was used to monitor the temperature of the copper tube which can be significantly higher than the output temperature of the salt mixture, particularly when the flow rate is low.

The flow was then varied in steps of 0.1 l/min and for each step the system was kept running for at least 5 min to reach stationary conditions.

In the next paragraph four data series are presented, at a flow rate ranging from 0.2 to 0.5 l/min. Another collection of data, in non-stationary conditions at lower flow rate, is reported, showing that the recommended maximum temperature for Hitec® can be



Fig. 9. The cavity receiver, built using a 6 mm copper pipe, before the oxidation process.



Fig. 10. The cavity receiver inserted into the insulated steel chamber and mounted on the collector. The black surface of the receiver obtained after the oxidization procedure of the Cu surface is visible.

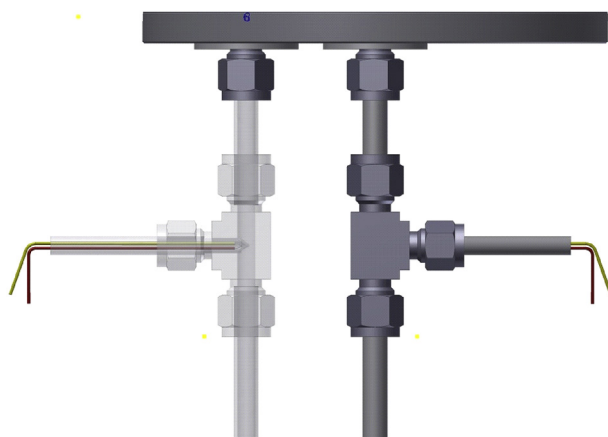


Fig. 11. Thermocouples at the inlet (left) and outlet (right) of the receiver. The three way Swagelok connector at the inlet and the steel support are represented as transparent to depict the exact position of the thermocouple.

reached in the present configuration.

5. Results and discussion

5.1. Temperatures of the molten salt mixture and the receiver

The temperature measurements, reported in Fig. 13, are referred to the inlet, outlet and back positions of the receiver for the four steady state flow rate conditions. Each test is referred to a time interval of 2 min. In Table 3 the mean values of the recorded data are reported.

Solar radiation was almost the same throughout the four measurements, while the salt temperature difference between inlet and outlet increases as the flow rate gets smaller. The difference in temperature between the inlet and the outlet is nearly inversely proportional to the flow, as shown in Fig. 14. In the same figure, the difference between the receiver and outlet temperature of salt is also reported. It is important to stress that the reported receiver temperature is only indicative (see description in section 3.6. Solar

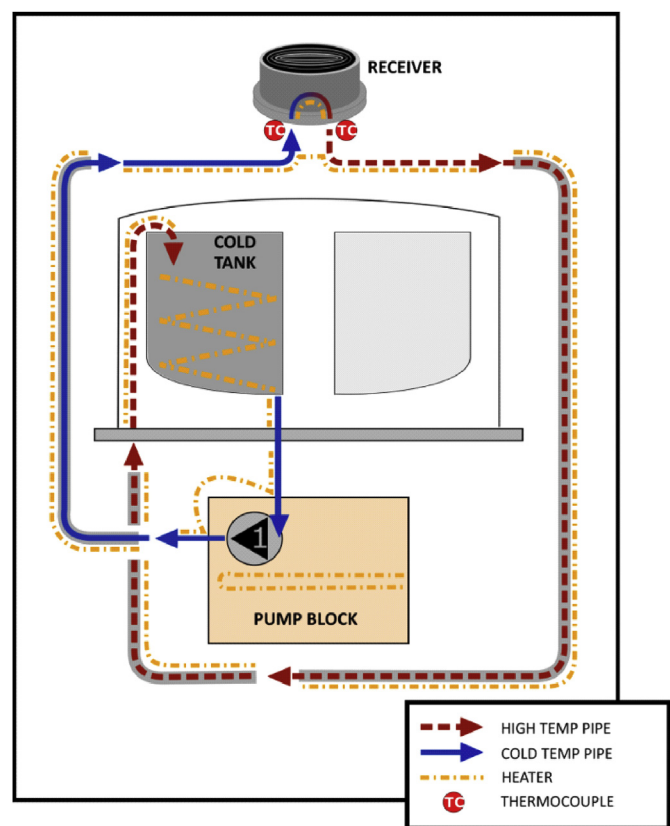


Fig. 12. Simplified arrangement for early field test of the receiver.

energy receiver) of the temperature of this component since it is based only on the monitoring of a single thermocouple. Due to this discrepancy, this temperature can be lower than the outlet temperature of the molten salts as happens for the case of high flow rate as evidenced also on Fig. 13.

The maximum temperature reached in stationary conditions is 415.8 °C, with a ΔT of 129.9 °C, while the receiver was at 449 °C.

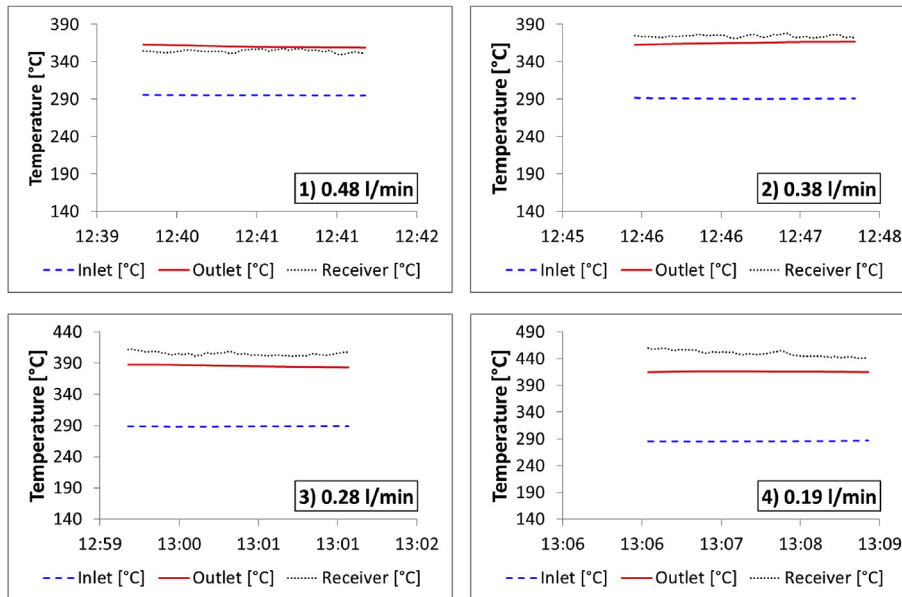


Fig. 13. Temperature measurements in 4 different flow conditions, inside the receiver and at its inlet and outlet.

We weren't able to establish stationary conditions with flow rates smaller than 0.2 l/min keeping an acceptable temperature in the receiver. A non-stationary data series is anyway presented in Fig. 15, since it demonstrates the maximum temperatures reached by the system. In particular, the Hitec® HTF reached a temperature of 540.8 °C, which is slightly above the maximum recommended operating temperature of Hitec® [21]; the temperature gain between the inlet and outlet was 271.3 °C, while the receiver temperature reached 712 °C.

In the first part of this data series the flow rate was lowered from 0.2 to 0.1 l/min but this led to an increase of the receiver temperature; the latter began to decrease only when the flow rate was set at 0.5 l/min.

This data series also shows the time lag in the temperature profiles throughout the transients: after the flow rate was set at 0.5 l/min, the outlet temperature kept increasing, reaching its maximum after about 20 s. This time lag is caused by the thermal inertia of the receiver and the thermocouples, and by the relatively low thermal conductivity of the molten salt mixture.

5.2. Energy analysis

An energy analysis was carried out to find the efficiency of the heat transfer to the molten salt in order to infer on the limit of our simple receiver.

The power of the solar radiation concentrated by the parabolic dish collector and delivered to the receiver can be expressed as:

$$P_D = \eta_D \cdot I_{dir} \cdot A_D \quad (2)$$

where η_D is the parabolic dish efficiency, which takes into account both the reflectivity properties of the mirror material and the shape errors of individual modules, I_{dir} is the direct solar irradiation and A_D is the total projected area of the three mirror sectors.

The concentrated solar radiation on the receiver is partly reflected, partly absorbed by the flowing molten salt mixture and partly lost due to convection and radiation. Power absorbed by the fluid is then given by:

$$P_R = m_{MS} \cdot C_{MS} \cdot (T_{OUT} - T_{IN}) = Q_{MS} \cdot \rho_{MS} \cdot C_{MS} \cdot (T_{OUT} - T_{IN}) \quad (3)$$

where m_{MS} is the mass flow rate of the molten salt, C_{MS} the average specific heat capacity, ρ_{MS} the average density, Q_{MS} the molten salt flow rate and T_{IN} and T_{OUT} are the temperatures at the inlet and outlet of the receiver, respectively. It must be underlined that ρ_{MS} is a linear function of the fluid temperature [21].

The thermal energy efficiency of the receiver is defined as the ratio of the power absorbed by the flowing molten salt to the concentrated solar power focused onto the receiver itself:

$$\eta_{REC} = \frac{P_R}{P_D} = \frac{Q_{MS} \cdot \rho_{MS} \cdot C_{MS} \cdot (T_{OUT} - T_{IN})}{\eta_D \cdot I_{dir} \cdot A_D} \quad (4)$$

Equation (4) is used to evaluate the heat absorbing capability of the solar receiver and depends on thermal losses, for both convection and radiation, and the thermal properties of the circulating

Table 3
Mean values of the data recorded at the four different flow rates: solar irradiance, inlet, outlet and receiver temperature. In the last column the difference ΔT between outlet and inlet temperature is reported.

	Measured flow rate [l/min]	Solar irradiance [W/m ²]	Inlet temp [°C]	Outlet temp [°C]	Receiver temp [°C]	ΔT [°C]
1	0.48	872.0	295.0	360.2	354.0	65.3
2	0.38	878.5	290.6	364.9	374.1	74.3
3	0.28	871.9	288.7	385.6	405.1	96.9
4	0.19	887.7	285.9	415.8	449.8	129.9

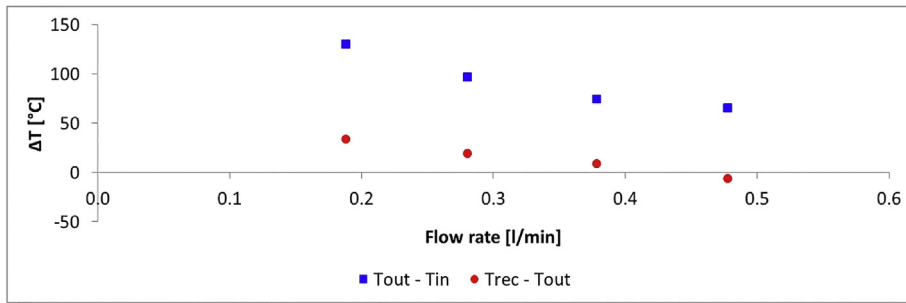


Fig. 14. Difference between outlet and inlet temperatures and difference between receiver and outlet temperature, for different flow rates.

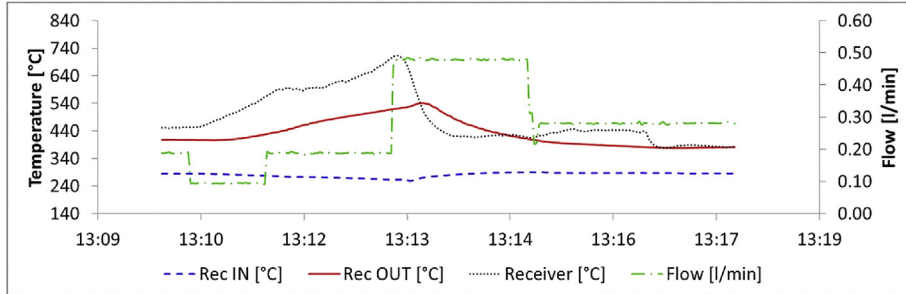


Fig. 15. 8 min data series, in non-stationary conditions, showing the maximum temperatures reached during the measurements.

molten salt. Also, since the dish prototype used in this experimentation is small, the flow must be kept low in order to reach high temperatures: this is expected to decrease efficiency, since convection and radiation losses impact consequently increases.

5.3. Uncertainty analysis

The receiver efficiency depends on Q_{MS} , T_{IN} , T_{OUT} and I_{dir} .

The temperature uncertainties $U_{T_{IN}}$ and $U_{T_{OUT}}$ were evaluated after calibration of the thermocouples by comparison with a PT100 sensor; flow rate and direct solar radiation uncertainties ($U_{Q_{MS}}$ and $U_{I_{dir}}$) are instrumental.

All these quantities are summarized in Table 4. Complex uncertainty was calculated with Eq. (5) and is found to be between 0.024 and 0.032.

Table 5

Mean power P_R absorbed by the molten salt and efficiency values calculated for the measurements at the four flow rates. Values of solar irradiance, gain in temperature ΔT between outlet and inlet of the receiver and concentrated solar radiation P_D are also reported.

	Measured flow rate [l/min]	Solar Irradiance [W/m ²]	ΔT [°C]	P_D [W]	P_R [W]	η_{REC}
1	0.48	872.0	65.3	1674	1283	0.77
2	0.38	878.5	74.3	1687	1158	0.69
3	0.28	871.9	96.9	1674	1114	0.67
4	0.19	887.7	129.9	1704	997	0.58

receiver, power absorbed by the molten salt and efficiency of the receiver were calculated using Eqs. (2)–(4). The calculated values are reported in Table 5. As expected thermal losses increase at low flow rates leading to the lowest receiver efficiency for the test at 0.19 l/min, see also Fig. 16.

$$U_{\eta_{REC}} = \sqrt{\left(\frac{\partial \eta_{REC}}{\partial Q_{MS}} \cdot U_{Q_{MS}}\right)^2 + \left(\frac{\partial \eta_{REC}}{\partial T_{OUT}} \cdot U_{T_{OUT}}\right)^2 + \left(\frac{\partial \eta_{REC}}{\partial T_{IN}} \cdot U_{T_{IN}}\right)^2 + \left(\frac{\partial \eta_{REC}}{\partial I_{dir}} \cdot U_{I_{dir}}\right)^2} \quad (5)$$

5.4. Collected power and efficiency

For each of the four measurements, power delivered to the

6. Conclusions

This work presents the preliminary results of the performances of a small prototype parabolic dish collector coupled with an innovative molten salt storage configuration.

The use of the Hitec molten salt (MS) mixture has been exploited to be used as high temperature carrier to cover wide temperature ranges. This has been achieved by selecting different MS flow rates and monitoring the inlet and outlet sections of the radiation receiver. The thermal efficiency of the proposed plant reaches values from 0.77 in correspondence to the highest flow rate (0.48 l/min, $T_{OUT} = 360.2$ °C) to 0.58 for the lowest value (0.19 l/min,

Table 4
Measurement uncertainties.

Inlet temperature,	<0.5 °C
Outlet temperature,	<0.5 °C
Direct solar irradiation,	<0.5%
Flow rate,	<4%

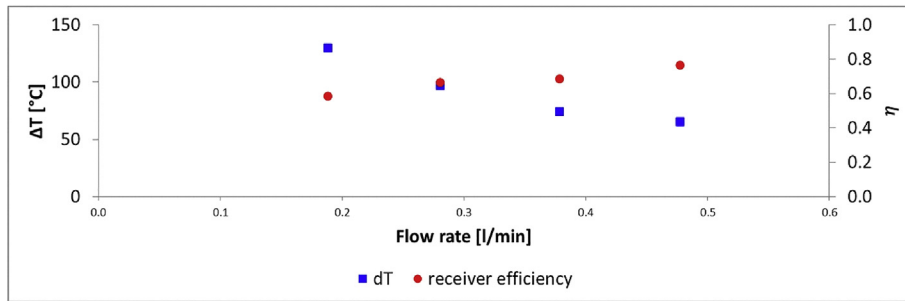


Fig. 16. Measured gain in temperature ΔT between outlet and inlet of the receiver and calculated efficiency of the receiver as a function of the flow rates.

$T_{OUT} = 415.8$.

The maximum output temperature of 540.8°C has been achieved in correspondence to transient test conditions and for MS flow rates below $0.2 \text{ l}/\text{min}$. The optimization of the receiver design has emerged as a major issue of the project since it has a relevant impact in enhancing the global efficiency of the process. The flexibility of the adopted configuration to work at different flow rates jointly with the possibility to make available the thermal power at ground level look like the more interesting benefits of the proposed solution. The experimental analysis required further assessments and the proposed results have to be considered part of a work in progress. In any case they look promising and encouraging for the implementation of this technology in view of its integration in the next distributed energy scenarios.

Acknowledgments

This work was partially supported by the PAT (Provincia Autonoma di Trento) project MATRAS and partially by the PAT in cooperation with Institute for Polymers, Composites and Biomaterials, National Research Council (CNR, Italy) through project ENAM (No. 220068/s116).

References

- [1] E. Oró, A. Gil, A. De Gracia, D. Boer, L.F. Cabeza, Comparative life cycle assessment of thermal energy storage systems for solar power plants, *Renew. Energy* 44 (2012) 166–173.
- [2] R. Singh, I.J. Lazarus, M. Souliotis, Recent developments in integrated collector storage (ICS) solar water heaters: a review, *Renew. Sustain. Energy Rev.* 54 (2016) 270–298.
- [3] A. Jamar, Z.A.A. Majid, W.H. Azmi, M. Norhafana, A.A. Razak, A review of water heating system for solar energy applications, *Int. Commun. Heat Mass Transf.* 76 (2016) 178–187, <https://doi.org/10.1016/j.icheatmastransfer.2016.05.028>.
- [4] D. Aidroos, H. Abdul, W. Zaidi, W. Omar, Historical development of concentrating solar power technologies to generate clean electricity efficiently – a review, *Renew. Sustain. Energy Rev.* 41 (2015) 996–1027, <https://doi.org/10.1016/j.rser.2014.09.008>.
- [5] Y. Tian, C.Y. Zhao, A review of solar collectors and thermal energy storage in solar thermal applications, *Appl. Energy* 104 (2013) 538–553, <https://doi.org/10.1016/j.apenergy.2012.11.051>.
- [6] J. Parthipan, R.B. Nagalingeswara, S. Senthilkumar, Design of one axis three position solar tracking system for paraboloidal dish solar collector, *Mater. Today: Proc.* 3 (2016) 2493–2500.
- [7] P.D. Malali, S.K. Chaturvedi, T. Abdel-Salam, Performance optimization of a regenerative Brayton heat engine coupled with a parabolic dish solar collector, *Energy Convers. Manag.* 143 (2017) 85–95.
- [8] L. Li, S. Dubowsky, A new design approach for solar concentrating parabolic dish based on optimized flexible petals, *Mech. Mach. Theory* 46 (2011) 1536–1548.
- [9] A.Z. Hafez, Ahmed Soliman, K.A. El-Metwally, I.M. Ismail, Solar parabolic dish Stirling engine system design, simulation, and thermal analysis, *Energy Convers. Manag.* 126 (2016) 60–75.
- [10] S. Pavlovic, A.M. Daabo, E. Bellos, V. Stefanovic, S. Mahmoud, R.K. Al-Dadah, Experimental and numerical investigation on the optical and thermal performance of solar parabolic dish and corrugated spiral cavity receiver, *J. Clean. Prod.* 150 (2017) 75–92.
- [11] A. Mawire, S.H. Taole, Experimental energy and exergy performance of a solar receiver for a domestic dish concentrator for teaching purposes, *Energy Sustain. Dev.* 19 (2014) 162–169.
- [12] G. Barreto, P. Canhoto, Modelling of a Stirling engine with parabolic dish for thermal to electric conversion of solar energy, *Energy Convers. Manag.* 132 (2017) 119–135.
- [13] D. Kalaiakatos, M. Cucumo, V. Ferraro, M. Mele, S. Cucumo, A. Miele, Performance of Dish-Stirling CSP system with dislocated engine, *Int. J. Energy Environ. Eng.* 8 (2017) 65–80, <https://doi.org/10.1007/s40095-015-0183-z>.
- [14] Y. Kadri, H. Hadj Abdallah, Performance evaluation of a stand-alone solar dish Stirling system for power generation suitable for off-grid rural electrification, *Energy Convers. Manag.* 129 (2016) 140–156.
- [15] K.C. Divya, J. Østergaard, Battery energy storage technology for power systems. An overview, *Elec. Power Syst. Res.* 79 (2009) 511–520.
- [16] A.A. Hawwash, Hamdy Hassan, Mahmoud Ahmed, S. Ookawara, Khalid Elfeky, Long-term thermal energy storage using thermochemical materials, *Energy Proced.* 141 (2017) 310–314.
- [17] W.D. Steinmann, D. Laing, R. Tamme, Development of PCM storage for process heat and power generation, *J. Sol. Energy Eng.* 131 (2009), 041009.
- [18] C.W. Robak, T.L. Bergman, A. Faghri, Economic evaluation of latent heat thermal energy storage using embedded thermosyphons for concentrating solar power applications, *Sol. Energy* 85 (2011) 2461–2473.
- [19] M. Liu, N.H. Steven Tay, S. Bell, M. Belusko, R. Jacob, G. Will, W. Saman, F. Bruno, Review on concentrating solar power plants and new developments in high temperature thermal energy storage technologies, *Renew. Sustain. Energy Rev.* 53 (2016) 1411–1432.
- [20] M. Abid, T.A.H. Ratlamwala, U. Atikol, Performance assessment of parabolic dish and parabolic trough solar thermal power plant using nanofluids and molten salts, *Int. J. Energy Res.* 40 (2016) 550–563, <https://doi.org/10.1002/er.3479>.
- [21] Coastal Chemical Co. LLC., HITEC® Heat Transfer Salt, 2009. <http://stoppingclimatechange.com/MSR-HITEC%20Heat%20Transfer%20Salt.pdf>.
- [22] Abengoa Solar, Development of Molten Salt Heat Transfer Fluid Technology for Parabolic Trough Solar Power Plants, AbengoaSolar, LLC, 2013.
- [23] S.S.M. Tehrani, R.A. Taylor, K. Nithyanandam, A.S. Ghazani, Annual comparative performance and cost analysis of high temperature, sensible thermal energy storage systems integrated with a concentrated solar power plant, *Sol. Energy* 153 (2017) 153–172.
- [24] E. González-Roubaud, D. Pérez-Osorio, C. Prieto, Review of commercial thermal energy storage in concentrated solar power plants: steam vs. molten salts, *Renew. Sustain. Energy Rev.* 80 (2017) 133–148.
- [25] M. Falchetta, D. Mazzei, T. Crescenzi, L. Merlo, Design of the Archimede 5 MW molten salt parabolic trough solar plant, in: Proc. 15th SolarPACES Conf., Berlin, Germany, 15–18 September 2009 paper 11608.
- [26] M. Medrano, A. Gil, I. Martorell, X. Potaü, L.F. Cabeza, State of the art on high-temperature thermal energy storage for power generation. Part2 – case studies, *Renew. Sustain. Energy Rev.* 14 (2010) 56–72.
- [27] T.H. Murphy, W.D. Otting, P.E. Frye, Solar dish concentrator with a molten salt receiver incorporating thermal energy storage, US Patent 7299633 B2 (2006).
- [28] A. Al-Alili, Y. Hwang, R. Radermacher, Review of solar thermal air conditioning technologies, *Int. J. Refrig.* 39 (2014) 4–22, <https://doi.org/10.1016/j.ijrefrig.2013.11.028>.
- [29] S. Danaei Kenarsari, Y. Zheng, Fast pyrolysis of biomass pellets using concentrated solar radiation: a numerical study, *J. Sol. Energy Eng.* 136 (2014) 41004, <https://doi.org/10.1115/1.4027266>.
- [30] U. Herrmann, D.W. Kearney, Survey of thermal energy storage for parabolic trough power plants, *J. Sol. Energy Eng.* 124 (2002) 145–152, <https://doi.org/10.1115/1.1467601>.
- [31] M. Bettonte, R.S. Brusa, A. Miotello, Method and Equipment for Producing a Solar Concentrator, 2010, EP 2 122 269 B1.
- [32] M. Eccher, S. Turrini, A. Salemi, M. Bettonte, A. Miotello, R.S. Brusa, Construction method and optical characterization of parabolic solar modules for concentration systems, *Sol. Energy* 94 (2013) 19–27, <https://doi.org/10.1016/j.solener.2013.04.028>.
- [33] A. Salemi, M. Eccher, A. Miotello, R.S. Brusa, Dense array connections for photovoltaic systems in concentration, *Prog. Photovolt. Res. Appl.* 19 (2011) 379–390, <https://doi.org/10.1002/pip.1040>.

- [34] M. Eccher, A. Salemi, S. Turrini, R.S. Brusa, Measurements of power transfer efficiency in CPV cell-array models using individual DC-DC converters, *Appl. Energy* 142 (2015) 396–406, <https://doi.org/10.1016/j.apenergy.2014.12.038>.
- [35] D. Kearney, U. Herrmann, P. Nava, B. Kelly, R. Mahoney, J. Pacheco, R. Cable, N. Potrovitz, D. Blake, H. Price, Assessment of a molten salt heat transfer fluid in a parabolic trough solar field, *J. Sol. Energy Eng.* 125 (2003) 170–176, <https://doi.org/10.1115/1.1565087>.
- [36] E.G. Bohlmann, Heat Transfer Salt for High Temperature Steam Generation, Oak Ridge, TN (United States), 1972, <https://doi.org/10.2172/4595737>.
- [37] A. Mao, J.H. Park, G.Y. Han, T. Seo, Y. Kang, Heat transfer characteristics of high temperature molten salt for storage of thermal energy, *Korean J. Chem. Eng.* 27 (2010) 1452–1457, <https://doi.org/10.1007/s11814-010-0260-1>.
- [38] R.G. Reddy, Novel Molten Salts Thermal Energy Storage for Concentrating Solar Power Generation, Tuscaloosa, 2013, <https://doi.org/10.2172/1111584>.
- [39] K. Vignarooban, X. Xu, A. Arvay, K. Hsu, A.M. Kannan, Heat transfer fluids for concentrating solar power systems - a review, *Appl. Energy* 146 (2015) 383–396, <https://doi.org/10.1016/j.apenergy.2015.01.125>.
- [40] J.W. Raade, D. Padowitz, Development of molten salt heat transfer fluid with low melting point and high thermal stability, *J. Sol. Energy Eng.* 133 (2011) 31013, <https://doi.org/10.1115/1.4004243>.